AADE-19-NTCE-070

Real-Time determination of the rheological properties of High Over-Balanced Drilling Fluid Using Artificial intelligence

Ibrahim H. Gomaa, Salaheldin Elkatatny, Abdulazeez Abdulraheem and Mohamed A. Mahmoud, King Fahd University of Petroleum and Minerals.

Abstract

Nowadays, oil industry turns to look for hydrocarbons in much more challenging locations such as mature depleted reservoirs and ultra-deep locations. The conventional high overbalance drilling may lead to some extreme problems in the cases of depleted and ultra-deep reservoirs. Using a special type of drilling fluid that capable of bridging along the walls of the well and withstands a high differential pressure is a novel solution for drilling depleted formations and ultra-deep wells securely. Drilling fluids properties of the high over-balanced water-based drilling fluid (HOBWBDF) such as plastic viscosity (PV), apparent viscosity (AV), flow behavior index (n) and consistency index (k) are very vital inputs in managing rig hydraulics, margins of surge and swab pressure, equivalent circulation density (ECD) and hole cleaning. Measuring drilling fluid rheological properties in the laboratory is a time-consuming job and depending on specific equipment such as mud balance and rheometer. That is why measuring these properties on the well site is carried out only twice a day.

The main goal beyond this work is to build novel empirical models that are capable of predicting the above-mentioned rheological properties of high over-balanced water-based drilling fluid (HOBWBDF) on real time. The models are built based on only two inputs which are the mud weight from the mud balance test and Marsh funnel viscosity measured by the Marsh funnel test. More than 1200 real field measurement points were used to feed an artificial neural network in order to develop these novel empirical models.

The developed models using ANN technique showed a high accuracy for predicting the different drilling fluid rheological properties. The obtained results show maximum average absolute percentage error (AAPE) less than 8 % with a correlation coefficient higher than 93%. The main advantages of these models are their inexpensiveness as there is no need for additional equipment to be added to the rig site. Moreover, these models would greatly help the drilling engineers to manage the ECD, surge and swab pressure and hole cleaning which in return will be reflected positively on the drilling performance.

Keywords; *mud rheology, high-overbalanced drilling, ultra-deep gas wells, artificial intelligence, artificial neural networks (ANN). Introduction*

Introduction

American Petroleum Institute (API) stated that the drilling fluids can be defined as circulating fluid designed to be used during the rotary drilling operations and perform some specific functions, Fink (2015). The mechanical and geological functions of the drilling fluids can be summarized as carrying the cuttings away from the bit, cooling and lubricating the drilling tools and the side walls of the well and creating a quick impermeable filter cake to seal-off all the porous formations as rapidly, effectively and permanently as possible. For heaving shaly intervals, drilling fluids are used to stabilize and support the formation in order to prevent them from flowing into the well. Moreover, drilling fluids are the main source for the high hydrostatic pressure needed for the overbalance drilling applied to hinder any fluids or solids from entering the formation as well as prevent the hydrocarbons flow towards the well, Abraham (1933), Rabia (2001), Bybee (2004) and Mahmoud et al. (2018). Drilling fluids have to be non-damaging to the porous strata containing the hydrocarbons, non-hazardous to the surroundings and the crew dealing with them and corrosion and wear-safe for the drilling equipment Caenn and Chillingar (1996) and Fink (2015) .

Both aqueous and non-aqueous drilling fluids are considered as non-Newtonian fluids. Since then, the viscosity of the drilling fluids depends on the applied shear rates at a specific temperature and pressure. In order to describe the behavior of the drilling fluids over a range of shear rates, rheological models are intensively used. These models provide some practical ways to predict the drilling fluids behavior under different pumping (pressure) conditions. The most commonly used rheological models are; Bingham Plastic Model, Power Law Model and Herschel-Bulkley (yield-power law [YPL]) model (Rabia 2001) and Abegunrin et al. (2016).

The rheological properties of the drilling fluid are some reflections of its physical and chemical characteristics. The main properties of the drilling fluid are measured and reported on a daily basis while drilling. The mud weight test and the Marsh funnel viscosity test are simple short-time tests that are frequently carried out in the field every 15- 20 minutes. Unlike the complete mud rheology tests which are considered much more tiresome, time-consuming, and carried out only twice per day. Properties such as mud weight (MW), Marsh funnel

viscosity (MF), plastic viscosity (PV), yield point (YP), flow behavior index (n) and flow consistency index (K) distinguish the character of each drilling fluid and considered the main inputs for the different rheological models. In addition, these different rheological properties are used to calculate rig hydraulics, surge and swab pressure profiles and hole cleaning efficiency.

Drilling fluid density or simply the mud weight (MW) is used principally to control the hydrostatic pressure (HP) exerted by the drilling fluid against the wellbore Akpabio et al. (2015). Marsh Funnel is one of the classical ways to measure the drilling mud viscosity in a simple and quick manner. It is a very simple and reliable way to have an indication about the fluid viscosity especially in field conditions Pitt (2000) and Almahdawi et al. (2014).

Plastic viscosity of the drilling fluid is a very vital parameter in the drilling operations. As the solid content of the drilling fluid increases, plastic viscosity increases in return. An increase in plastic viscosity leads to an increase in the equivalent circulation density (ECD), surge and swab pressures and hence a higher possibility for differential sticking problem. On the other hand, plastic viscosity increase will lead to a reduction in the ROP Kersten (1946) and Paiaman et al. (2009). Adams and Charrier (1985) stated that the attractions between the solid antiparticles of the drilling fluid determine its yield point (YP). It was also mentioned that chemical dispersants, thinners and viscosifiers can control the drilling fluid yield point (YP).

The power law that is used to describe the behavior of the pseudo plastic fluids is used to represent the performance of the drilling fluid. This law can be described by Eq. (1);

$$Shear\ stress = K\ (shear\ rate)^n \quad (1)$$

Where (K) is called the fluid consistency index and (n) is the flow behavior index.

Viscosity value of the drilling fluid is directly proportional to the K value as K value can represent the thickness of the fluid. The higher the K, the higher the fluid viscosity. The flow behavior index (n) is used to describe the degree of fluid deviation away from the standard Newtonian behavior. In other words, n is used to represent the degree of the fluid non-Newtonian behavior. For the drilling fluids that act according to the pseudo plastic fluids behavior, the standard value of n is between zero and 1. Where the value is 1 for Newtonian fluids behavior and less than 1 for dilatant fluids. Gray et al. (1980)

High Over-Balanced Water-Based Drilling Fluid

Nowadays, oil industry turns to look for hydrocarbons in much more challenging locations such as mature depleted reservoirs and ultra-deep locations. The conventional high overbalance my lead to some extreme problems in the cases of depleted and ultradeep reservoirs. Problems such as lost circulation and stuck pipe are most probably encountered while drilling through depleted reservoirs. Due to the very low pore pressure in the depleted formation in the reservoirs, drilling a well to a specific target without damaging the formation is not possible Santos et al. (2003).

The conventional solution of this problem is to use an additional casing string to isolate the depleted/low pressure formation. However, this solution is costly and may be not applicable in some cases where the well diameter has reached its lower limit. Another more applicable solution to this is to use a special type of drilling fluid that capable of bridging along the walls of the well and withstands a high differential pressure. Figure (1) shows the mechanism of a high overbalance bridging mud that capable of tolerating a very high differential pressure in depleted reservoirs and through high porous and permeable formations with potentially high pore pressure. Using this (HOBWBDF) will secure the drilling operations whether above or through the target reservoir section as illustrated by Figure (1).

The main goal of this research is to create an empirical correlation models using artificial neural network (ANN) that is capable of predicting the rheological properties of this type of drilling fluid (HOBWBDF) in a real-time using the most frequent measured mud weight and Marsh funnel viscosity.

The Prediction of mud parameters of (HOBWBDF) at a real time will help in calculating the drilling hydraulics with high accuracy in real time, predicting the surge and swab pressure profiles, getting a continuous indication for the efficiency of hole cleaning and acquiring the ability to predict and cure different drilling problems like pipe sticking. Using only the measured mud weight and Marsh funnel viscosity as inputs for this model makes it a very field applicable one. The mud weight test and the Marsh funnel viscosity test are simple short-time tests that are frequently carried out in the field every 15- 20 minutes. Unlike the complete mud rheology tests that are considered much more tiresome, time-consuming, and carried out twice per day only.

Artificial intelligence applications in oil industry

McCarthy (2007) defined artificial intelligence (AI) as the technique of designing computer programs that enable the machines to act intelligently the same way as human being. AI can make analysis of big data that human brains cannot handle and interpret the different trends in order to make a forecast for future possibilities in no time and effort. This, in return, reduces the cost and errors associated with different operations as well as enhances their efficiency. The AI applications in the oil and gas filed is so abundant in all the industry aspects. Popa and Cassidy (2012) and Bello et al. (2015) agreed on the fact that the first applications of AI in the oil industry go back to the early 1990s.

Artificial neural networks (ANN) is a branch from the AI science. ANN can be considered as an emulation for the human neural system as it can be used to mimic the human intelligent attitudes Nakamoto (2017). In addition to simple linear problems, ANN is capable of finding a solution for complicated non-linear problems. The main consisting element of an ANN is called neuron. Each ANN must contain at least three main layers. The first layer represents the inputs and is called the input layer. The second layer, which could be subdivided into more than one layer, is called the hidden layer. The final layer represents the outputs and is called the output layer. The data is trained within the ANN throughout a training function such as (trainlm,trainbr,.. etc). At the same time, data is transferred

from the hidden layer to the output layer throughout a transfer function. The most common transfer functions are hardlim, purelin and logsig functions. Figure (2), illustrates the general schematic of the ideal ANN Demuth et al. (2016).

Doraisa et al. (1998) examined the possibility of using artificial neural networks (ANN) as a tool for optimizing field development plans. Lim and Kim (2004) used the fuzzy logic technique to determine some reservoir properties like porosity and permeability from well logs. The generated model showed a better estimation for the predicted data more than the previously used computer methods. Ozbayoglu and Ozbayoglu (2009) used both ANN backpropagation and Jordan/Elman techniques for the determination of frictional pressure losses (FPL) and flow patterns (FP) with high accuracy up to 0.005 mean square error (MSE).

Elkatatny and Mahmoud (2017) used the ANN (white box) for the first time to predict the oil formation volume factor. Their model showed a tremendous accuracy with R^2 of 0.997 and AAPE of less than 1%. Mahmoud et al. (2017) developed an empirical correlation using ANN model to determine the (TOC) of the Barnett and Devonian shales. The produced correlation showed a high accuracy with R^2 of 0.93 and 0.89 for Barnett and Devonian shale respectively.

Since the issue of determining the mud rheological properties has a great importance in the drilling field, So many researchers tried to implement the applications of AI for predicting the various properties of drilling fluids. Osman and Aggour (2003) used ANN backpropagation technique to predict the density of both OBM and WBM. The model input parameters were initial mud density at surface conditions, temperature, pressure and drilling fluid type. Razi et al. (2013) used the feed-forward multilayer perceptron (FFMLP) neural network to predict the rheological properties of water base mud (WBM). Shear rate, temperature and concentration were used as model inputs. Adesina et al. (2015) worked on the prediction of the downhole density for some environmentally friendly OBM such as Diesel, Jatropha and Canola. The authors used temperature only as an input for their model. Elkatatny et al. (2016) and Elkatatny (2017) used the ANN technique to intensively predict the mud rheological properties for different types of drilling fluids such as KCl water based drilling fluid and invert emulsion drilling fluid.

For the high-overbalanced water-based drilling fluid (HOBWBDF), it will be the first time to develop models capable of predicting the rheological properties of this kind of drilling fluid.

Methodology

More than 1200 data points of the measured mud weight (MW) of the high overbalance drilling fluid along with the measured Marsh funnel time viscosity (MF), measured plastic viscosity (PV) and measured yield point (YP) are used for developing and validating the ANN model. The data points come in the field units which are pound per cubic foot (PCF) for the mud weight, sec/quart for the Marsh funnel viscosity, cP for the plastic viscosity and lb/100 ft^2 for the yield point. A sample of the data is available in the Table (1).

Since this data set is coming from the field where the human measurement error is very common and the efficiency of mud separation system controls a lot of measured mud properties, the data has to be filtered first. The filtration process was based on removing the out-scaled data points and the values that do not follow the physical concepts that the drilling fluids obey.

The viscometer readings R_{300} and R_{600} were calculated from the YP and PV values based on the following Eqs. (2 & 3). Then, the flow behavior index (n) could be calculated through Eq. (4), Savins and Roper (1954)

$$R_{300} = YP + PV \quad (2)$$

$$R_{600} = PV + R_{300} \quad (3)$$

$$n = 3.32 * \log\left(\frac{R_{600}}{R_{300}}\right) \quad (4)$$

Data statistical analysis

Data statistical analysis was carried out to determine the minimum, maximum, mean, range, standard deviation, skewness and kutosis of the data that will be used. The results of this analysis is shown in Table (2). Mud weight varies between 64-155 (PCF), Marsh funnel viscosity varies between 42 -120 (sec/quart), plastic viscosity varies between 9-63 (cP), yield point varies between 15 -65 (lb./100ft2), flow behavior index (n) varies between 0.32-0.76, flow consistency index (k) varies between 0.54-4.84, R_{300} values vary between 35-125 (rpm) and finally, R_{600} values vary between 44-185 (rpm). The data range and arithmetic mean can also be found in Table (2).

In order to determine the relation between the input and output data, correlation coefficient analysis was carried out and the results are shown in figure (3). The results show that almost all the mud rheological parameters have a stronger relationship with the mud weight than the Marsh funnel viscosity.

Building the empirical models

The final data set was divided into 70% for the model training and the rest 30% for the model validation and testing. About 500 combinations of the data were tried to reach the optimum data sets for both training and testing. Different combinations of the number of neurons and the number of hidden layers were tried to achieve the minimum average absolute percentage error (AAPE), the highest correlation coefficient (R) and the highest coefficient of determination (R^2) between the target and output data. Several training and transfer functions were examined using the MATLAB toolbox.

Once the desired results are attained, the network is saved and its weights and biases are extracted. Using the saved network structure and the resulting weights and biases, the final empirical model is established in order to reproduce the same results without the need to use the original network again.

Results and discussion

The ANN model used to predict the mud viscometer reading at 300 rpm (R_{300}) contained only one hidden layer with 22 neurons. The training function used was “trainlm” with a transfer function of “tansig”. The AAPE of the training and the testing process are 2.86% and 3.70% respectively. While the data shows a perfect match with a correlation coefficient (R) of 0.98 and 0.97 for training and the testing respectively, see

figures (4 & 5).

Since the transfer function used is the "tansig" function, all the inputs are normalized by the network between -1 and 1 according to Eq. (5). So, therefore, after extracting the weights and biases from the network, this normalization should be reversed again to find the denormalized (original) value of the output.

$$X_{n\,(-1:1)} = 2\left(\frac{X - X_{min}}{X_{max} - X_{min}}\right) - 1 \quad (5)$$

The extracted weights and biases for the R_{300} model can be found in Table (3). Using these values of the weights and biases, the mathematical model for predicting the viscometer reading R_{300} can be constructed by Eq. (6). In order to reverse the normalization occurred by Eq. (6) The denormalized R_{300} values could be found from Eq. (7).

$$R_{300\_n} = \left[\sum_{i=1}^{N} W2_i \left(\frac{2}{1 + e^{-2\left(W1_{i,1}\,MW_n + W1_{i,2}\,MF_n + b1_i\right)}} - 1\right)\right] + b_2 \quad (6)$$

$$R_{300} = 45.483 * R_{300_n} + 87.483 \quad (7)$$

Where, R_{300_n}, MW_n and MF_n are the normalized values of R_{300}, MW and MF respectively. N is the optimized total number of neurons, W_1 is the optimized weight between the inputs and the hidden layer, b_1 is the bias optimized for the hidden layer, W_2 is the optimized weight for the output layer and b_2 is its optimized bias.

For the R_{600} prediction, almost the same ANN model parameters for R_{300} were used. The network consisted of one single hidden layer with 22 neurons. The "trainlm" function used as a data training function while the "tansig" function used as a transfer function. The AAPE of the training and the testing process are 3.5% and 4.80% respectively. While the model comes with a high correlation coefficient (R) between the actual and the predicted values of R_{600} of 0.98 and 0.96 for the training and testing sets respectively, see figures (6 & 7).

Since the transfer function for the R_{600} model is the "tansig" function, the final model could be constructed using the extracted network optimized weights and biases on the form of Eq. (8). The extracted weights and biases for the R_{600} are shown in Table (4). Use Eq. (9) to obtain the denormalized (original) value of R_{600}.

$$R_{600\_n} = \left[\sum_{i=1}^{N} W2_i \left(\frac{2}{1 + e^{-2\left(W1_{i,1}\,MW_n + W1_{i,2}\,MF_n + b1_i\right)}} - 1\right)\right] + b_2 \quad (8)$$

$$R_{600} = 65.728 * R_{600_n} + 117.991 \quad (9)$$

Plastic viscosity values (PV) were predicted using the ANN model which give a high correlation coefficient of 0.96 and 0.94 for the training and testing stages respectively. The AAPE of the training and testing respectively were 5.6% and 7.7% only. See figures (8 &9). The emperical model that is based on the extracted weights and biases of the ANN to calculate PV can be described by Eq. (11). The coefficients for Eq. (10) can be found in Table (5). The final denormalized value of PV can be calculated from Eq. (11).

$$PV_n = \left[\sum_{i=1}^{N} W2_i \left(\frac{2}{1 + e^{-2\left(W1_{i,1}\,MW_n + W1_{i,2}\,MF_n + b1_i\right)}} - 1\right)\right] + b_2 \quad (10)$$

$$PV = 25.935 * PV_n + 35.5089 \quad (11)$$

Another critical rheological parameter which is the flow behavior index (n) was successfully predicted using only the mud weight and Marsh funnel viscosity by the ANN technique. Almost the same model parameters used for the prediction of R_{300} and R_{600} were used for the prediction of (n). The model comes with a high correlation coefficient (R) between the actual and the predicted values of (n) of 0.93 and 0.94 for the training and testing sets respectively. The AAPE of 2.5% for both training and testing, see figures (10 & 11).

The emperical model that is based on the extracted weights and biases of the ANN to calculate (n) can be described by Eq. (12). The coefficients for Eq. (12) can be found in Table (6). The final denormalized value of PV can be calculated from Eq. (13).

$$n_n = \left[\sum_{i=1}^{N} W2_i \left(\frac{2}{1 + e^{-2\left(W1_{i,1}\,MW_n + W1_{i,2}\,MF_n + b1_i\right)}} - 1\right)\right] + b_2 \quad (12)$$

$$n = 0.2183 * n_n + 0.5403 \quad (13)$$

An ANN model was developed following the same procedures of the above-mentioned models to predict the apparent viscosity (AV) from both mud density and Marsh funnel time. The model shows a high accuracy for predicting the value of AV. The correlation coefficient (R) between the original and predicted (AV) values is 0.98 for all the data set (training and testing) with AAPE of only 3.96% see figure (12) The mathematical model derived from the ANN for calculating the AV can be described by Eq. (14). The coefficient of Eq. (14) can be found in Table (7). For denormalizing the values of (AV), we may use Eq. (15).

$$AV_n = \left[\sum_{i=1}^{N} W2_i \left(\frac{2}{1 + e^{-2\left(W1_{i,1}\,MW_n + W1_{i,2}\,MF_n + b1_i\right)}} - 1\right)\right] + b_2 \quad (14)$$

$$AV = 31.224\,AV_n * +58.889 \quad (15)$$

Model Validation:

The developed ANN models can be validated by predicting the value of fluid flow consistency index (k) by using Eq. (16). The predicted (k) values which are considered based on the ANN models of (R_{600}) and (n) show a good match with the actual calculated (k) values with root mean square error (RMSE) of 0.18 only as shown in figure (13).

$$K = \frac{R^*_{600}}{1022^{n^*}} \quad (16)$$

Where R^* and n^* are the predicted values of R600 and (n) using ANN technique.

This validation proves the accuracy and applicability of the developed ANN model to acquire the different mud rheological properties of the high-overbalance fluid like plastic viscosity, apparent viscosity, yield point, fluid flow index and consistency index. All these different outputs could be obtained using the devolved model at real time using only the frequently measured mud weight and Marsh funnel viscosity.

Conclusions

In this research, an ANN technique was used to generate empirical models that are capable of predicting the rheological parameters of high-overbalance drilling fluid at a real time. The models inputs are more than 1200 real field measured points of mud weight and Marsh funnel viscosity. The highest AAPE for all the predicted parameters was only 7.7% and the least correlation coefficient was as high as 0.93. This proves the high capability of ANN to efficiently predict the rheological parameters of the (HOBWBDF).

Using these models with the (HOBWBDF) will make the drilling of ultra-deep wells that penetrate high porous depleted formations go smoothly without so much interrupting drilling problems. Since this developed model is not expensive and does not require any additional requirement, it will be so practical and helpful for the drilling engineers to use it in the rig site.

Acknowledgments

I would like to provide my thanks and appreciation for Dr. Abdulazeez Abdulraheem for providing all the knowledge required for the use of the artificial intelligence techniques. I should also thank all the co-authors for their support and technical help.

All appreciation goes to College of Petroleum and Geosciences, King Fahd University of Petroleum and Minerals for providing the essential software and materials required to produce this work.

References

1. Abegunrin, O. A., S. O. Okhuevbie, and I. L. Animasaun. 2016. "Comparison between the Flow of Two Non-Newtonian Fluids over an Upper Horizontal Surface of Paraboloid of Revolution: Boundary Layer Analysis." Alexandria Engineering Journal **55** (3): 1915–29. https://doi.org/10.1016/j.aej.2016.08.002.
2. Abraham, W. E. V. 1933. "The Functions of Mud Fluids Used in Rotary Drilling". Presented in the 1st World Petroleum Congress, 18-24 July, London, UK. https://goo.gl/sePuVj
3. Adams, Neal, and Tommie Charrier. 1985. Drilling Engineering: A Complete Well Planning Approach. Tulsa, Okla: PennWell Pub. Co.
4. Adesina, Fadairo A. S., Adeyemi Abiodun, Ameloko Anthony, and Falode Olugbenga. 2015. "Modeling the Effect of Temperature on Environmentally Safe Oil Based Drilling Mud Using Artificial Neural Network Algorithm." Petroleum & Coal 57 (1): 60–70.
5. Akpabio, Julius U., P. N. Inyang, and C. I. Iheaka. 2015. "The Effect of Drilling Mud Density on Penetration Rate." IRJET 2 (9): 29–35.
6. Almahdawi, F. H., Al-Yaseri, A. Z, and Jasim, N. 2014. Apparent Viscosity Direct from Marsh Funnel Test. Iraqi Journal of Chemical and Petroleum Engineering 15 (1): pp. 51-57.
7. Bello, Opeyemi, Javier Holzmann, Tanveer Yaqoob, and Catalin Teodoriu. 2015. "Application Of Artificial Intelligence Methods In Drilling System Design And Operations: A Review Of The State Of The Art." Journal of Artificial Intelligence and Soft Computing Research 5 (2): 121–39. https://doi.org/10.1515/jaiscr-2015-0024.
8. Caenn, Ryen, and George V. Chillingar. 1996. "Drilling Fluids: State of the Art." Journal of Petroleum Science and Engineering 14 (3): 221–230. https://doi.org/10.1016/0920-4105(95)00051-8.
9. Demuth, Howard, Mark Beale, and Martin Hagan. 2016. "Neural Network ToolboxTM 6", version 4. The MathWorks, Inc.
10. Doraisa, H, T. Ertekin, and A.S. Grader. 1998. "Key Parameters Controlling the Performance of Neuro-Simulation Applications in Field Development." SPE-51079-MS presented at the SPE Eastern Regional Meeting, 9-11 November, Pittsburgh, Pennsylvania.
11. Elkatatny, Salaheldin, and Mohamed Mahmoud. 2017. "Development of New Correlations for the Oil Formation Volume Factor in Oil Reservoirs Using Artificial Intelligent White Box Technique." Petroleum 4 (2): 178–86. https://doi.org/10.1016/j.petlm.2017.09.009.
12. Elkatatny, Salaheldin, Zeeshan Tariq, and Mohamed Mahmoud. 2016. "Real Time Prediction of Drilling Fluid Rheological Properties Using Artificial Neural Networks Visible Mathematical Model (White Box)." Journal of Petroleum Science and Engineering 146 (October): 1202–10. https://doi.org/10.1016/j.petrol.2016.08.021.
13. Elkatatny, Salaheldin. 2017. "Real-Time Prediction of Rheological Parameters of KCl Water-Based Drilling Fluid Using Artificial Neural Networks." Arabian Journal for Science and Engineering 42 (4): 1655–65. https://doi.org/10.1007/s13369-016-2409-7.
14. Fink, Johannes. 2015. Petroleum Engineer's Guide to Oil Field Chemicals and Fluids, 2nd ed. Gulf Professional Publishing, Elsevier. https://doi.org/10.1016/C2015-0-00518-4.
15. Gray, G. R, Darley, H. C. H and Rogers, W. F. 1980. Composition and Properties of Oil Well Drilling Fluids. Houston, Texas: Gulf Publ.
16. Kersten, G.V., 1946. "Results and Use of Oil-Base Fluids in Drilling and Completing Wells". Paper API-46-61 presented at Drilling and Production Practice, New York, 1 January.
17. Lim, Jong-Se, and Jungwhan Kim. 2004. "Reservoir Porosity and Permeability Estimation from Well Logs Using Fuzzy Logic and Neural Networks". Paper SPE-88476-MS presented at SPE Asia Pacific Oil and Gas Conference and Exhibition, 18-20 October, Perth, Australia. https://doi.org/10.2118/88476-MS.
18. Mahmoud, Ahmed Abdulhamid A., Salaheldin Elkatatny, Mohamed Mahmoud, Mohamed Abouelresh, Abdulazeez

Abdulraheem, and Abdulwahab Ali. 2017. "Determination of the Total Organic Carbon (TOC) Based on Conventional Well Logs Using Artificial Neural Network." International Journal of Coal Geology 179 (June): 72–80. https://doi.org/10.1016/j.coal.2017.05.012.

19. Mahmoud, Omar, Hisham A. Nasr-El-Din, Zisis Vryzas, and Vassilios C. Kelessidis. 2018. "Using Ferric Oxide and Silica Nanoparticles To Develop Modified Calcium Bentonite Drilling Fluids." *SPE Drilling & Completion* 33 (01): 12–26. https://doi.org/10.2118/178949-PA.
20. McCarthy, J., 2007. What Is Artificial Intelligence? Computer Science Department, Stanford University, Stanford, CA 94305. http://www-formal.stanford.edu/jmc
21. Nakamoto, P., (2017) "Neural networks and deep learning: deep learning explained to your granny—a visual introduction for beginners who want to make their own deep learning neural network (machine learning), first ed. CreateSpace Independent Publishing Platform
22. Osman, E. A., and M. A. Aggour. 2003. "Determination of Drilling Mud Density Change with Pressure and Temperature Made Simple and Accurate by ANN". Paper SPE-81422-MS, Presented at Middle East Oil Show, 9-12 June, Bahrain. https://doi.org/10.2118/81422-MS.
23. Ozbayoglu, E. M., and M. A. Ozbayoglu. 2009. "Estimating Flow Patterns and Frictional Pressure Losses of Two-Phase Fluids in Horizontal Wellbores Using Artificial Neural Networks." Petroleum Science and Technology 27 (2): 135–49. https://doi.org/10.1080/10916460701700203.
24. Paiaman, A M, M K Ghassem Al-Askari, B Salmani, B D Al-Anazi, and M Masihi. 2009. "Effect of Drilling Fluid Properties on Rate of Penetration." NAFTA 60 (3): 129–34.
25. Pitt, M. J. 2000. "The Marsh Funnel and Drilling Fluid Viscosity: A New Equation for Field Use." SPE Drilling & Completion 15 (01): 3–6. https://doi.org/10.2118/62020-PA.
26. Popa, Andrei Sergiu, and Stephen David Cassidy. 2012. "Artificial Intelligence for Heavy Oil Assets: The Evolution of Solutions and Organization Capability." In SPE Annual Technical Conference and Exhibition, 8-10 October, San Antonio, Texas, USA.
27. Rabia, H. 2001. Well Engineering and Construction. Entrac Consulting.
28. Razi, Meisam Mirarab, Mohammad Mazidi, Fatemeh Mirarab Razi, Hamed Aligolzadeh, and Shahram Niazi. 2013. "Artificial Neural Network Modeling of Plastic Viscosity, Yield Point, and Apparent Viscosity for Water-Based Drilling Fluids." Journal of Dispersion Science and Technology 34 (6): 822–27. https://doi.org/10.1080/01932691.2012.704746.
29. Santos, H.M., Shayegi, S. and leuchtenberg, C., Microflux Control: The Next Generation in Drilling Process for Ultradeep Water; Paper OTC 15062 presented at the 2003 Offshore Technology Conference, Houston, TX, 5-8 May 2003.
30. Bybee, Karen. 2004. "Drilling Fluid Strengthens Wellbore." *Journal of Petroleum Technology* 56 (11): 59–60. https://doi.org/10.2118/1104-0059-JPT.

Appendix

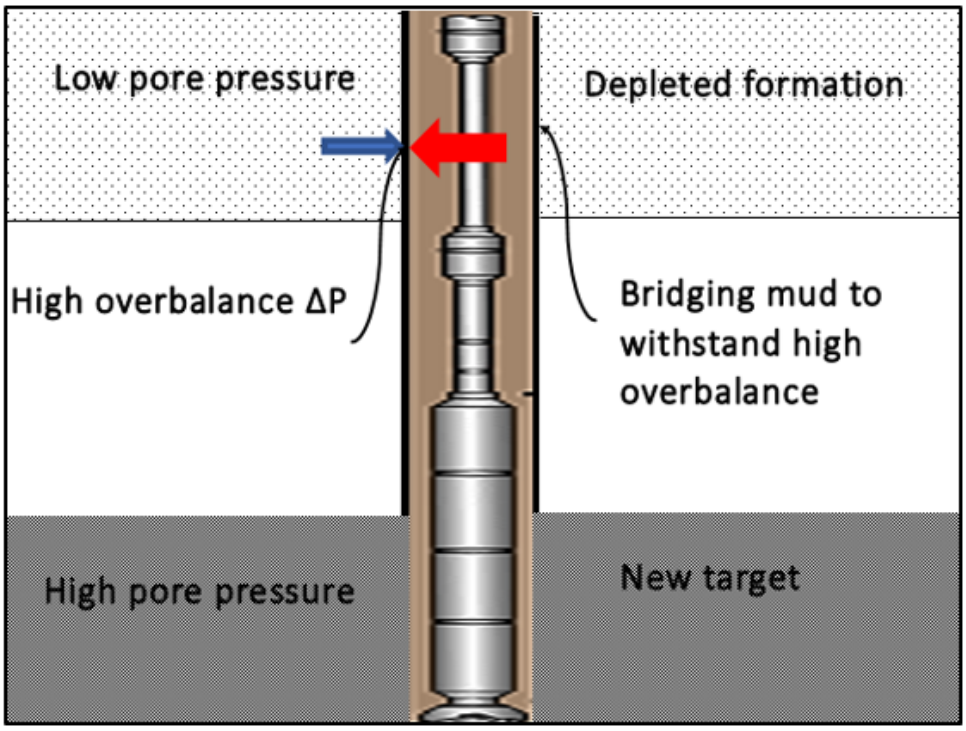

Figure 1: Drilling through depleted formations using (HOBWBDF)

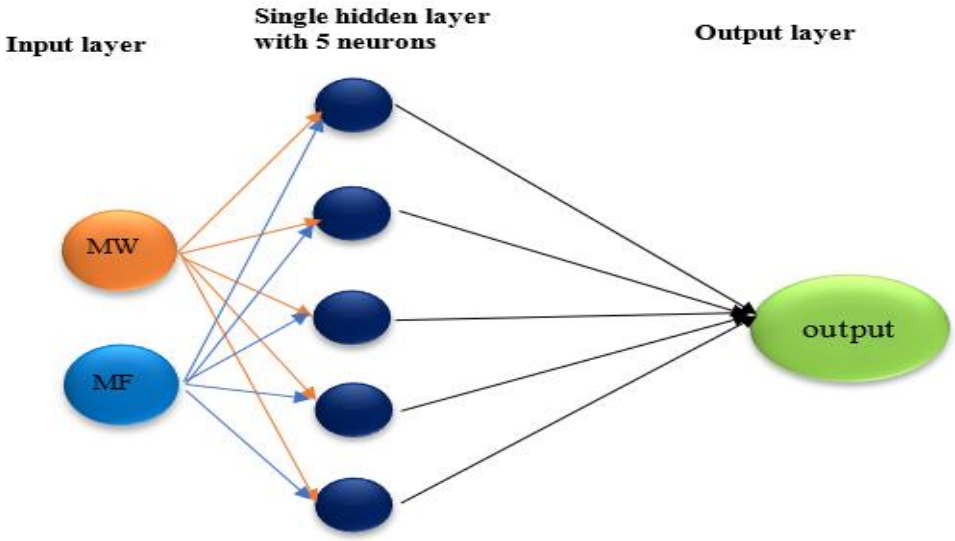

Figure 2 Illustration scheme for an ideal ANN with single hidden layer

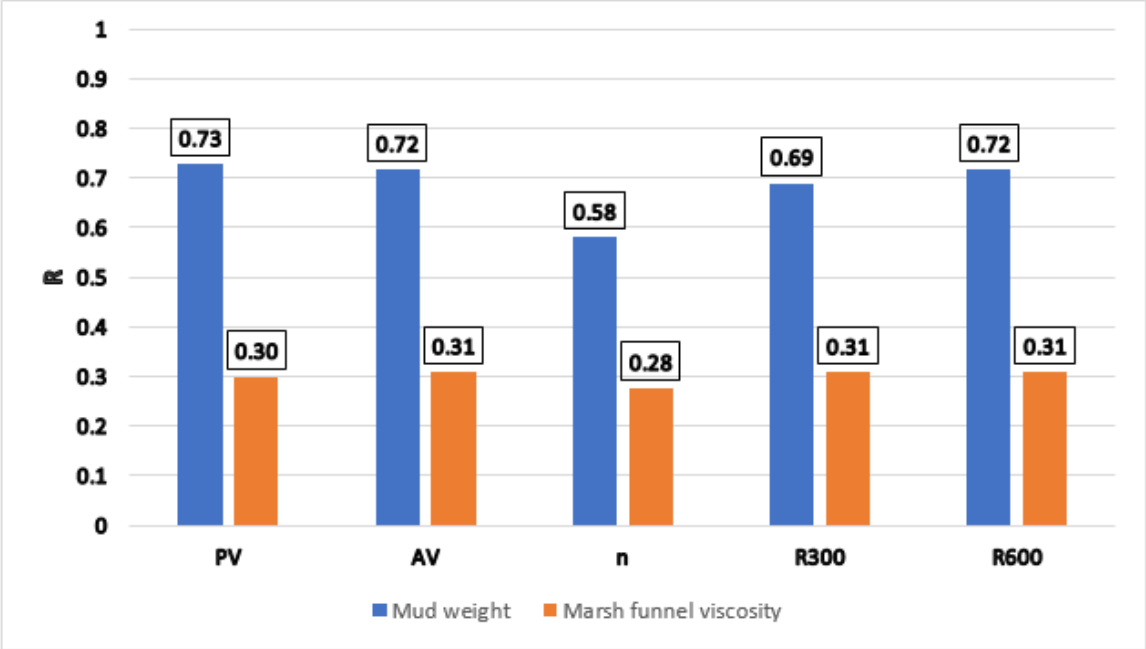

Figure 3 Correlation coefficients between inputs and outputs

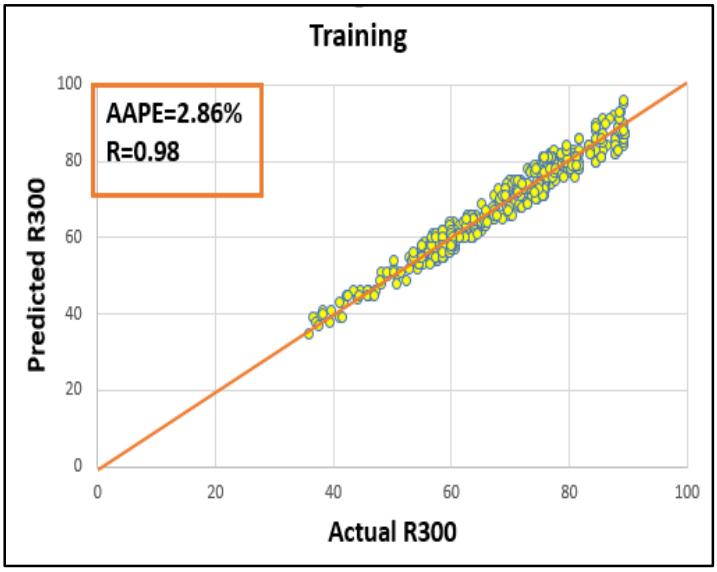

Figure 4: The relation between the actual and predicted R300 (Training stage)

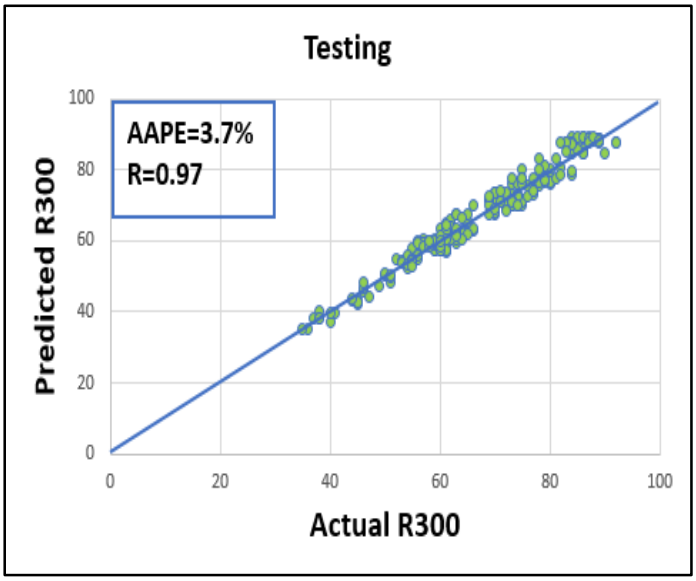

Figure 4: The relation between the actual and predicted R300 (Testing stage)

Figure 6: The relation between the actual and predicted R600 (Training stage)

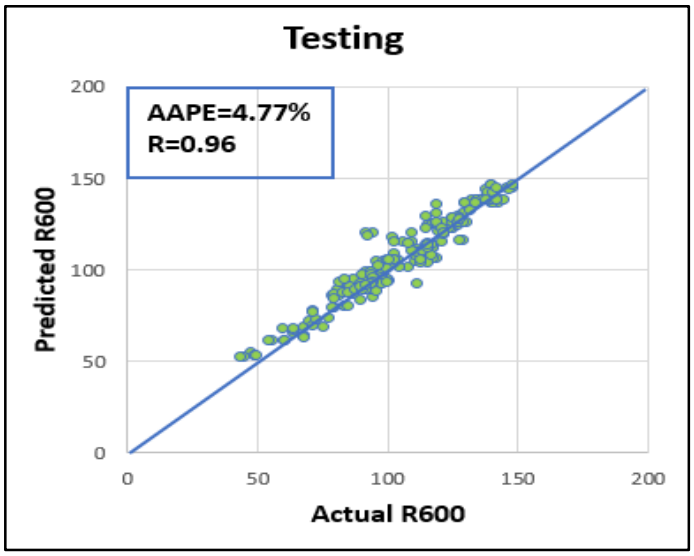

Figure 7: The relation between the actual and predicted R600 (Testing stage)

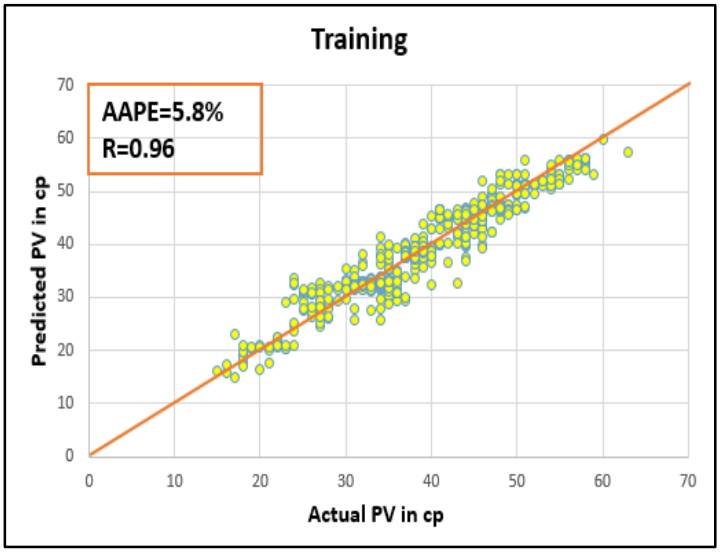

Figure 8: The relation between the actual and predicted PV (Training stage)

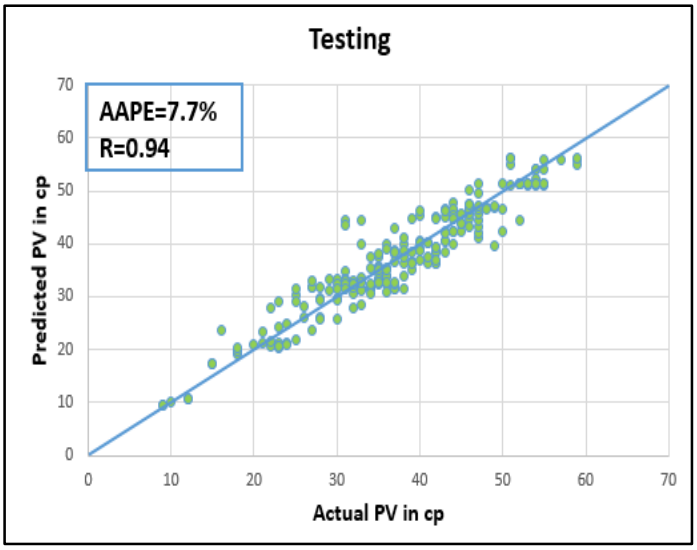

Figure 9: The relation between the actual and predicted PV (Testing stage)

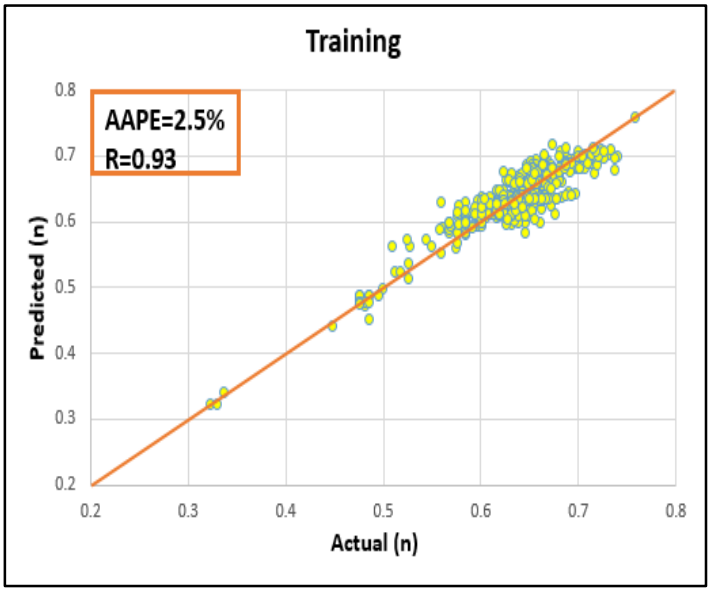

Figure 10 The relation between the actual and predicted (n) factor (Training stage)

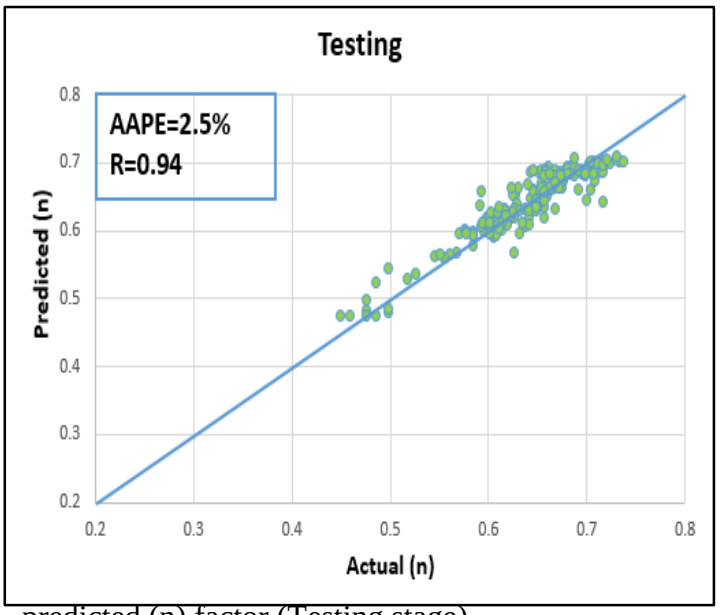

predicted (n) factor (Testing stage)

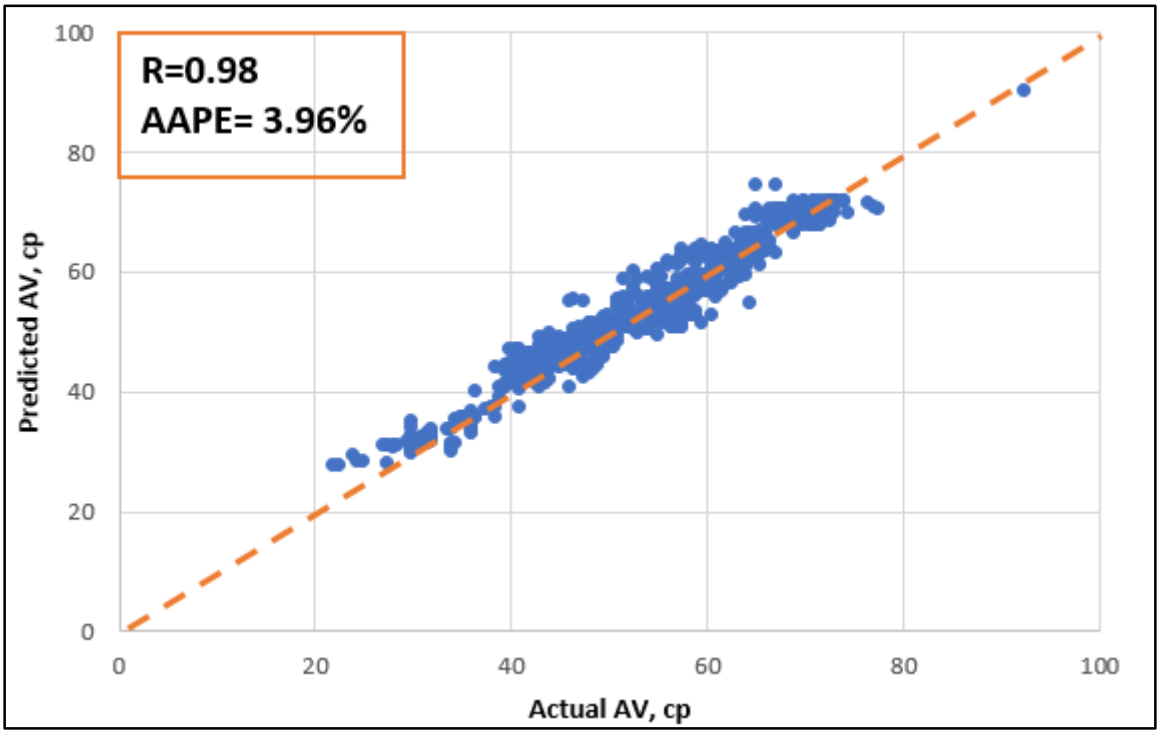

Figure 12 The comparison between the actual and predicted (AN) values using ANN model for both training and testing data

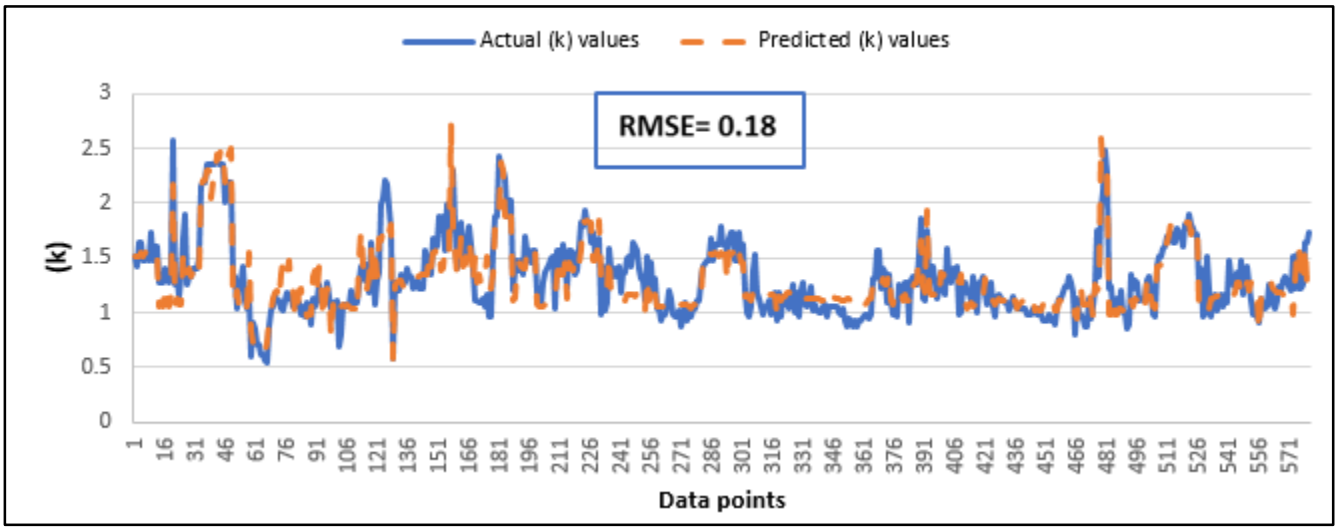

Figure 13 the comparison between the actual and predicted (k) values with RMSE of 0.18

Table 1 Sample of field data for High-overbalanced water-based drilling fluids (total of 1263 data points).

Mud Density, lb/ft^3	Funnel Viscosity, sec/quart	Plastic Viscosity, cP	Yield Point, lb/100 ft^3
70	47	17	27
76	48	18	28
78	48	18	27
87	48	20	37
89	60	26	28
90	66	38	33
93	55	32	26
100	85	34	30
105	67	38	27
120	74	47	37

Table 2 Statistical analysis of the High-overbalanced water-based drilling fluid data

	MW	MF	PV	YP	n	k	R_{300}	R_{600}
min	64.00	42.00	9.00	15.00	0.32	0.54	35.00	44.00
max	155.00	120.00	63.00	65.00	0.76	4.84	125.00	185.00
arithmetic mean	110.47	62.85	38.11	30.04	0.63	1.37	68.15	106.26
range	91.00	78.00	54.00	50.00	0.44	4.30	90.00	141.00

standard deviation	22.79	9.93	10.11	4.69	0.06	0.52	12.78	22.56
Skewness	0.15	0.44	-0.14	0.30	-1.25	2.29	-0.06	-0.10
Kurtosis	1.75	4.17	2.60	7.06	5.33	11.57	2.84	2.58

Table 3 Coefficients for R_{300}, Eq. (6)

Hidden Layer Neurons (N)	**Weight Between Inputs and Hidden Layer (W_1)**		**Hidden Layer Biases (b_1)**	**Weight Between Output and hidden Layer (W_2)**	**Output Layer Biases (b_2)**
	1	**2**			
1	4.098504	4.896601	-6.83719	1.024568	-0.388
2	-4.20754	5.35171	5.390523	-0.25181	
3	3.463057	-5.05282	-6.06654	-0.30987	
4	-6.66745	2.245366	4.645837	0.379793	
5	-5.62864	2.791305	2.385475	-0.3678	
6	-0.97671	7.426166	3.866751	0.046326	
7	-2.9753	-5.61467	2.881258	-1.23436	
8	1.665418	-5.38846	-1.27591	1.063036	
9	-2.23461	7.376363	1.672297	0.702791	
10	-3.52824	-0.0558	-0.35922	1.022886	
11	5.073362	5.036049	0.932776	-0.8721	
12	3.252689	-5.88784	0.995759	0.055886	
13	9.226587	0.740876	2.87064	0.588285	
14	4.024253	5.671599	3.189117	1.977344	
15	-2.74324	-5.21002	-1.01249	-0.19142	
16	6.137072	5.20283	0.870462	0.838781	
17	6.919352	4.924533	5.889454	0.556071	
18	-7.50653	-3.20921	-4.65171	0.797103	
19	-5.01807	-7.46349	-4.16148	1.426024	
20	4.576175	-4.57061	4.809655	1.013717	
21	-4.96351	4.186576	-5.8989	-0.622	
22	-4.50142	-6.29802	-8.59083	-0.23875	

Table 4 Coefficients for R600 Eq. (8)

Hidden Layer Neurons (N)	Weight Between Inputs and Hidden Layer (W_1)		Hidden Layer Biases (b_1)	Weight Between Output and hidden Layer (W_2)	Output Layer Biases (b_2)
	1	2			
1	4.121	4.901	-6.807	0.514	0.341
2	-4.974	3.480	6.141	-0.847	
3	2.109	-5.479	-5.627	-1.593	
4	-7.239	3.944	3.086	-0.596	
5	-4.170	4.887	4.075	-1.200	
6	-1.700	8.815	3.181	-1.124	
7	-5.083	-3.476	1.439	1.032	
8	2.719	-5.020	-3.452	-1.431	
9	-1.534	7.210	2.513	1.509	
10	-4.425	3.708	1.260	-0.572	
11	5.103	4.812	-0.508	0.504	
12	3.184	-4.801	0.044	0.028	
13	6.690	-1.337	1.967	0.463	
14	4.057	5.941	2.642	0.742	
15	-2.678	-5.554	-2.594	0.785	
16	6.334	0.425	0.195	-0.742	
17	4.997	5.236	4.587	0.907	
18	-9.357	-3.250	-5.476	0.842	
19	-1.387	-6.128	-3.940	0.269	
20	7.218	-2.910	4.351	0.252	
21	-4.787	4.398	-6.378	0.791	
22	-0.213	-6.311	-6.927	0.475	

Table 5 Coefficients for PV Eq. (10)

Hidden Layer Neurons (N)	Weight Between Inputs and Hidden Layer (W_1)		Hidden Layer Biases (b_1)	Weight Between Output and hidden Layer (W_2)	Output Layer Biases (b_2)
	1	2			
1	4.079	4.898	-6.851	0.308	0.611
2	-3.695	6.454	5.691	-1.283	
3	1.890	-4.632	-3.843	-1.415	
4	-7.111	4.031	3.660	-0.790	
5	-3.326	5.070	4.229	0.532	
6	-2.088	9.197	3.317	-1.156	
7	-5.326	-3.619	1.225	0.969	
8	2.910	-6.390	-1.865	0.750	
9	-2.202	7.477	2.460	1.976	
10	-5.865	3.640	0.988	-0.191	
11	5.521	5.933	-0.279	0.478	
12	2.231	-5.230	0.254	0.057	
13	7.016	-1.396	2.140	0.394	
14	4.852	4.667	2.997	-0.164	
15	-3.571	-5.613	-2.276	-0.574	
16	6.212	1.269	0.627	-0.476	
17	5.583	4.463	4.257	1.354	
18	-8.825	-3.880	-5.498	1.207	
19	-3.482	-6.816	-3.316	0.453	
20	6.705	-3.903	3.799	0.217	
21	-4.791	4.486	-6.451	1.244	
22	-0.289	-7.094	-6.282	-0.172	

Table 6 Coefficients for "n" Eq. (12)

Hidden Layer Neurons (N)	Weight Between Inputs and Hidden Layer (W_1)		Hidden Layer Biases (b_1)	Weight Between Output and hidden Layer (W_2)	Output Layer Biases (b_2)
	1	2			
1	5.109	4.094	-6.580	0.645814	0.1802
2	-4.830	5.734	7.493	1.686524	
3	-2.406	4.021	4.637	-2.66526	
4	7.867	-0.158	-3.755	-0.85947	
5	-1.608	-6.354	4.073	0.408485	
6	3.414	5.542	-3.728	0.051887	
7	-4.016	-4.986	3.435	0.249771	
8	8.003	1.054	-2.579	1.523527	
9	-3.554	3.178	0.507	-1.69304	
10	-5.373	-4.110	0.955	-0.20372	
11	5.508	1.448	-1.092	-1.46176	
12	10.067	-2.986	0.243	-1.05758	
13	6.747	0.180	1.735	0.731758	
14	5.824	-0.869	1.788	-1.57417	
15	4.404	-3.299	2.180	1.041844	
16	2.768	5.853	1.751	0.367618	
17	-3.621	-9.563	-6.210	-0.44991	
18	1.333	-6.633	3.532	-1.01984	
19	-4.423	-6.231	-5.580	0.996064	
20	2.732	2.325	3.265	4.076742	
21	-6.527	-1.040	-5.286	2.233129	
22	0.412	-6.462	6.657	0.402873	

Table 8 Coefficients for AV Eq. (14)

Hidden Layer Neurons (N)	Weight Between Inputs and Hidden Layer (W_1)		Hidden Layer Biases (b_1)	Weight Between Output and hidden Layer (W_2)	Output Layer Biases (b_2)
	1	2			
1	3.997	4.899	-6.933	0.875832	0.108
2	-5.260	4.547	5.730	0.27323	
3	0.810	-4.920	-4.189	0.280995	
4	-5.370	3.882	4.294	-0.98946	
5	-6.552	3.560	4.657	0.685235	
6	-1.255	7.408	3.860	0.132406	
7	-6.610	-2.276	3.285	0.704341	
8	2.626	-5.489	-2.958	-0.35442	
9	-2.171	7.149	1.844	0.316494	
10	-3.646	3.741	1.891	-0.52779	
11	3.423	4.076	-1.522	0.779755	
12	1.329	-3.234	-1.023	1.05767	
13	4.252	-5.120	1.575	0.043673	
14	4.645	4.969	2.457	0.149744	
15	-2.621	-6.504	-2.003	-0.20726	
16	6.743	-0.765	0.161	-0.7113	
17	8.236	2.566	4.525	-0.7422	
18	-7.499	-1.318	-2.695	-0.48219	
19	-5.274	-5.279	-5.029	-0.49451	
20	5.226	-4.400	5.003	0.915248	
21	-4.817	3.797	-6.474	0.507709	
22	-0.268	-7.216	-5.841	-0.38506	